Sinusoidal magnetic structure in a three-dimensional antiferromagnetic $Co_2(OH)AsO_4$: Incommensurate-commensurate magnetic phase transition

I. de Pedro,[1,2] J. M. Rojo,[2] J. Rodríguez Fernández,[1] M. T. Fernández-Díaz,[3] and T. Rojo[2,*]
[1]*CITIMAC, Facultad de Ciencias, Universidad de Cantabria, 39005 Santander, Spain*
[2]*Departamento de Química Inorgánica, Facultad de Ciencia y Tecnología, Universidad del País Vasco, 48080 Bilbao, Spain*
[3]*Institut Laue-Langevin, BP 156X, F-38042 Grenoble Cedex, France*
(Received 26 December 2009; revised manuscript received 10 March 2010; published 23 April 2010)

$Co_2(OH)AsO_4$ has been prepared by hydrothermal synthesis and characterized from x-ray and neutron powder diffraction. The structure consists of a three-dimensional framework in which $Co(1)O_5$-trigonal bipyramid dimers and $Co(2)O_6$-octahedra chains are simultaneously present. The magnetic structure has been determined by neutron (D2B and D1B) powder-diffraction data. Below 22 K, the $Co_2(OH)AsO_4$ phase shows an incommensurate antiferromagnetic structure along the *b* direction. The propagation vector $(0,\delta,0)$ is temperature dependent with a value of $\delta=0.430$ at the lowest temperature (1.8 K). Magnetization measurements of $Co_2(OH)AsO_4$ show a complex magnetic behavior with the presence of three different signals. Between 6 and 21 K, a strong dependence of the magnetic field is observed with a shift of the inflexion point associated to the three-dimensional antiferromagnetic ordered from 18 K at 1 kOe to 20.1 K at 90 kOe. The small splitting observed in the zero-field-cooled-field-cooled curves at low temperatures is characteristic of ferromagnetic interactions but saturation is not reached even up to 90 kOe. Heat-capacity measurements show an unusual dependence on the magnetic field for antiferromagnetic transitions with a jump at the Neél temperature quite small (2 J/Kmol). The magnetic contribution exhibits a λ-type anomaly associated to the three-dimensional antiferromagnetic ordering. Surprisingly, the λ anomaly grows with the magnetic field and becomes better defined. Neutron powder diffraction in different fields shows a magnetic phase transition. The incommensurate magnetic structure evolves at low temperatures toward a collinear AF phase for fields higher than 35 kOe.

DOI: 10.1103/PhysRevB.81.134431 PACS number(s): 75.30.Kz, 61.05.fm

I. INTRODUCTION

In the last years, the compounds showing a "metal-insulator" transition have attracted much attention in solid-state physics and chemistry since the discovery of additional fascinating magnetic phenomena. Many cobalt-based compounds present this type of phenomenology, such as the magnetic frustration system, $Ca_3Co_2O_6$,[1] which shows in the magnetically ordered state a ferromagnetic coupling between the magnetic ions along the chains whereas the interchain nearest-neighbor interaction is antiferromagnetic (AF). Other Co-based systems with spin state $S=3/2$ show a three-dimensional (3D) Neel ordering at low temperature, with unusually large magnetic anisotropy such as $BaCo_2Si_2O_7$,[2] $CoNb_2O_6$,[3] CoV_2O_6,[4]and $BaCo_2V_2O_8$.[5] Moreover, in some cases, they present also interesting field-induced magnetic transitions. For example, a spin-flop transition in $CoNb_2O_6$ (Ref. 3) and an order-disorder transition in $BaCo_2V_2O_8$ (Ref. 6) have been described.

In the case of the phosphate and arsenate cobalt compounds, additional useful chemical and physical properties (magnetic, heterogeneous catalysis, ion exchange, etc.)[7–10] have been found out. The stoichiometries and a wide variety of structural types built of interconnected MO_6 (M=Ti,V,Cr,Fe,Mo,…) octahedra and XO_4 (X=P,As) tetrahedra make them an appropriate domain to study the relationships between the physical properties and the crystal packing features.[7,8]

The crystal structure of the $Co_2(OH)XO_4$ (X=P,As) (Refs. 11–13) compounds consists of condensed network of a vertex and edge-sharing CoO_6, CoO_5 y XO_4 subunits (see Fig. 1). The Co(II) ions can be sited in two different octahedral and trigonal bipyramidal topologies. The edge-sharing $[Co(2)O_4(OH)_2]$ octahedra give rise to linear chains propagated along the *c* axis whereas the edge-sharing $[Co(1)O_4(OH)]$ trigonal bipyramids constitute dimeric entities. The chain of octahedra, the dimeric unites, and the tetrahedral groups share corners thereby forming a three-dimensional network.

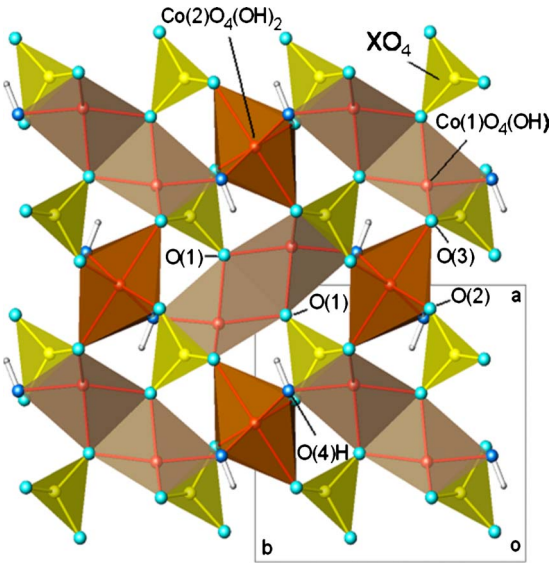

FIG. 1. (Color online) Projection of the crystal structure of $Co_2(OH)XO_4$ (X=P and As) along the [001] direction.

We have recently discovered in the hydroxy phosphate $Co_2(OH)PO_4$ (Ref. 11) the coexistence of antiferromagnetic ordering and a spin-glass behavior in an insulator compound. In this phase, a magnetic frustration in the Co(1) magnetic moments is observed as due to the presence of antiferromagnetic interactions between Co(2) neighbor chains. Furthermore, it is worth mentioning the existence of a superexchange angle Co(1)-O(3)-Co(2) with a value of 107° that involves ferromagnetic couplings between chain and dimer neighbors ferromagnetically coupled. This exchange angle was the higher angle found in the literature for a ferromagnetic exchange pathway and plays an interesting role in the magnetic behavior of this system.[11] The partial substitution of transition-metal ions in the structure severely affects the magnetic properties[14,15] giving rise to the evolution of the 3D antiferromagnetic system in the $Co_{2-x}Cu_x(OH)PO_4$ solid solution[15] up to a spin-gap system in the $Cu_2(OH)PO_4$ phase,[16] the spin-glasslike state in the $(Co,Ni)_2(OH)PO_4$ detected below 10 K,[14] or the higher ferromagnetic interactions at lower temperatures in $Co_{1.7}Mn_{0.3}(OH)PO_4$ coexisting with a similar spin-glass state observed in the nonsubstituted cobalt hydroxy phosphate.[17]

The similar ability of AsO_4^{3-} and PO_4^{3-} tetrahedra to stabilize anionic frameworks and the greater size of the AsO_4^{3-} anions predict some differences in the crystal packing features that could modify the complex magnetic properties exhibited in these phases. In this work, we present a deeper magnetic study of $Co_2(OH)AsO_4$ in order to determine (i) the nature of the main magnetic interactions and their anomalies, (ii) the magnetic structure of the low-temperature ordered phase, and (iii) the magnetic variations with respect to the isostructural $Co_2(OH)PO_4$ compound. Magnetostructural correlations of these cobalt (II) phases are also described.

II. EXPERIMENTAL

A. Synthesis

Hydrothermal techniques have been used to prepare the $Co_2(OH)AsO_4$ synthetic phase in the laboratory. This arsenate has been found in the nature as a solid solution with adamite $Zn_2(OH)AsO_4$ mineral.[18,19] Our synthetic pathway to obtain a pure cobalt phase begins with the preparation of the $Co_3(AsO_4)_2 \cdot 8H_2O$ precursor, which was previously described.[20] Due to the low solubility of the Co(II) hydrated arsenates, long reaction times and pH values in the 6–8 range were needed. Approximately 0.2 g of the hydrated precursor were disgregated in 35 ml of water and placed in a Teflon-lined stainless-steel autoclave under autogeneous pressure generated by a temperature of approximately 170 °C.

The contents of Co and As were determined by inductively coupled plasma atomic emission spectroscopy performed with an ARL Fisions 3410 spectrometer, confirming the $Co_2(OH)AsO_4$ chemical formula. The thermogravimetric study was performed up to 800 °C under air in a Perkin-Elmer TGA-DSC System 7 thermobalance. The decomposition curve reveals an initial (~1%) weight loss associated with water absorbed on the surface from the atmosphere and at 660 °C a second step (~3.5%) attributed to the loss of water obtained from the decomposition of 2 f.u. At temperatures above 700 °C, additional weight losses were not observed on the thermogravimetric curve. These results are in good agreement with those obtained in other hydroxy phosphate and arsenate-related compounds.[11,12,14]

B. X-ray and neutron powder-diffraction experiments

Room temperature x-ray powder-diffraction data of microcrystalline purple samples were used to evaluate the purity of the $Co_2(OH)AsO_4$ product. The data were collected in the $10° \leq 2\theta \leq 90°$ range in steps of 0.02° with an integration time of 16 s per step using a Philips X'Pert-MPD x-ray diffractometer with secondary beam graphite monochromated Cu $K\alpha$ radiation. The $Co_2(OH)AsO_4$ data were fitted using the pattern matching routine of the program FULLPROF,[21] in an orthorhombic cell with the *Pnnm* space group as previously determined by Keller *et al.*[13] The x-ray refined unit-cell parameters $a=8.281(1)$, $b=8.566(1)$, $c=6.038(1)$ Å, $\alpha=\beta=\gamma=90°$, $V=429.4(1)$ Å^3, and $Z=4$ are close to those reported [$a=8.286(2), b=8.594(2), c=6.051(1)$ Å, $V=430.9$ Å^3, $Z=4$] from single-crystal data.[13] No extra diffraction peaks were observed, concluding that the synthetic products correspond to a pure phase which will be used in the study of the magnetic properties.

Neutron powder-diffraction measurements were performed on the D1B and D2B powder diffractometers at the Institute Laue-Langevin (ILL) of Grenoble. About 5 g of $Co_2(OH)AsO_4$ were employed in the experiments, placed in a cylindrical vanadium container and held in a liquid-helium cryostat. The high resolution of D2B (1.5938 Å) was used to obtain extensive and accurate structural data at room temperature and 2 K respectively, over a large angular angle $0° \leq 2\theta \leq 150°$. The structure determined by using x-ray single-crystal data of cobalt hydroxy arsenate[13] was used as a starting model for the refinements. High flux and medium resolution of D1B at 2.525 Å were used to study the thermal evolution of the sample in the temperature range 1.8–50 K to solve the magnetic contributions of the neutron patterns. The diffraction patterns were collected every 2 K and 25 min in the angular range $10° \leq 2\theta \leq 90°$. The Rietveld method[22] was used to refine simultaneously the nuclear and magnetic structures. All the patterns were analyzed using the FULLPROF program suite.[21] The background was fitted using the polynomial refinable function and a pseudo-Voigt function was chosen to generate the line shape of the diffraction peaks. The D1B patterns were refined sequentially, taking as starting parameters of each pattern those resulting from the refinement of the proceeding one.

C. Magnetic measurements

dc magnetic-susceptibility measurements of powdered samples were performed using Quantum Design (QD) physical property measurement system-superconducting quantum interference device magnetometers whilst heating from 2 to 300 K in different applied magnetic from 1 to 90 kOe, after cooling in either the presence (field cooling, FC) or the absence (zero-field cooling, ZFC) of the applied field. Magne-

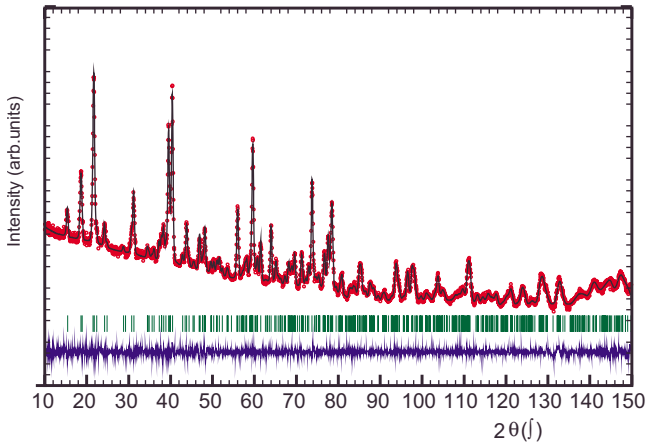

FIG. 2. (Color online) Observed (circles), calculated (solid line), and difference (at the bottom) neutron-diffraction (D2B, ILL) profiles for $Co_2(OH)AsO_4$ at room temperature. Vertical marks correspond to the position of the allowed reflections for the crystallographic structure.

tization as a function of field (H) was measured using a standard QD PPMS magnetometer in the $-90 \leq H/\mathrm{kOe} \leq 90$ range in the temperature range of 2–20 K after cooling the sample in zero field. ac magnetic-susceptibility measurements were performed using the same QD PPMS system with an alternate excitation field (H_{ac}) of 10 Oe and a frequency of 1000 Hz. Field-dependent data were collected from 2 to 60 K at a fixed frequency of 1000 Hz with applied fields from 0 to 90 kOe.

Heat capacity has been measured between 1.8 and 300 K with a standard relaxation method using a two-tao model. In order to guarantee a good thermal contact, apiezon N grease was used to glue the sample to the sample holder. The addenda (sample holder plus grease) was measured at different magnetic fields before the sample measurements and then subtracted from the total heat capacity in order to get the sample heat capacity. The sample was an 11.2 mg plate obtained compressing the original thin powder.

III. RESULTS

A. Nuclear structure

The structural refinements of $Co_2(OH)AsO_4$ were carried out from high-resolution neutron powder-diffraction patterns (D2B) recorded at room temperature with $\lambda = 1.5938$ Å. The Rietveld refinement was fitted in the *Pnnm* space group and cell parameters reported for a single-crystal specimen by Keller *et al.*[13] as starting point. It should be noted that the quality of our results permits the localization of the hydrogen ions in the structure. The experimental, calculated, and difference neutron powder-diffraction profiles are shown in Fig. 2. There is no significant mismatch between the observed intensity and the calculated profile. The room-temperature structural parameters and the reliability factors from D2B data refinements are summarized in Table I. The final refined positional and thermal parameters are given in Table II. The main interatomic distances, angles for $Co_2(OH)AsO_4$ are listed in Table III.

TABLE I. Details of Rietveld full-profile refinement from D2B neutron powder-diffraction pattern at room temperature for $Co_2(OH)AsO_4$.

Compound	$Co_2(OH)AsO_4$
Space group	*Pnnm* (No. 58)
a (Å)	8.2587(2)
b (Å)	8.5801(1)
c (Å)	6.0391(1)
V (Å^3)	427.94(3)
Instrument	D2B (ILL)
Radiation (Å)	1.5938
Monochromator	Ge (335)
Z	4
2θ range (deg)	0–150
2θ step-scan increment (deg)	0.05
No. of reflections	433
No. of profile parameters	26
Reliability factors (%)	
$R_P = \Sigma\lvert y_{i,obs} - (1/c)y_{i,calc}\rvert / \Sigma y_{i,obs}$	16.6
$R_{WP} = [\Sigma w_i \lvert y_{i,obs} - (1/c)y_{i,calc}\rvert^2 / \Sigma w_i [y_{i,obs}]^2]^{1/2}$	14.4
$R_B = [\Sigma\lvert I_{obs} - I_{cal}\rvert] / \Sigma I_{obs}$	8.14
χ^2	1.68

The crystal structure of the $Co_2(OH)AsO_4$ phase can be described as formed by two crystallographically distinct sites for the metal ions (see Fig. 3). Co(1) is fivefold coordinated by oxygen atoms in approximately trigonal-pyramidal geometry where one of the apical positions is occupied by an OH group. Co(2) exhibits a distorted octahedral geometry with two long apical Co(2)-O(3) bonds and four shorter equatorial links, two of which are hydroxide groups in *cis* configuration (see Table III). The axial and equatorial O-Co(2)-O mean angles in the $Co(2)O_6$ octahedra are 171° and 87°, respectively. The octahedra sharing the O(2)-O(2) and the O(4)H-O(4)H edges give rise to linear chains propagated along the z axis. For the $Co(1)O_5$ polyhedra, each trigonal bipyramid exhibits three set of O-Co(1)-O angles around 95°, 123°, and an axial to 165°. In addition, the trigonal bipyramids constitute dimeric entities, sharing the O(1)-O(1) edge (see Fig. 3). Both sublattices, Co(2) chains and Co(1) dimers are cross linked via oxygen [O(3), O(4)H] bridges.

In the $Co_2(OH)AsO_4$ phase, the arsenate groups exhibit three different bond lengths and four different bond angles where mean distances and angles are 1.69(1) Å and 109(5)°, respectively. The As-O values and O-As-O angular regions show that the AsO_4 tetrahedra are fairly regular as in the majority of the adamite-type $M_2(O/OH)XO_4$ compounds. This fact could affect the magnetic properties of the transition-metal arsenate compounds due to the degree of distortion of the $M(2)O_4(OH)_2$ octahedra and $M(1)O_4(OH)$ trigonal bipyramidal geometries. Finally, the chain of octahedral, the dimeric unites, and the arsenate anions share corners, thereby forming a three-dimensional framework, resulting in a condensed structure without any identifiable channels or pores. The bond distances and angles obtained

TABLE II. Final refined positional and thermal parameters from the neutron-diffraction pattern (D2B) at room temperature for $Co_2(OH)AsO_4$.

Atom	Site	x	y	z	B_{iso} (Å^2)
Co(1)	4*g*	0.362(1)	0.368(1)	0.5	0.3(1)
Co(2)	4*f*	0.5	0	0.252(1)	0.6(1)
As	4*g*	0.2480(4)	0.2479(5)	0	0.5(3)
O(1)	4*g*	0.1022(5)	0.1068(4)	0	0.70(7)
O(2)	4*g*	0.4253(4)	0.1463(5)	0	0.66(6)
O(3)	8*h*	0.2282(3)	0.3637(3)	0.2233(3)	0.41(4)
O(4)	4*g*	0.3906(5)	0.1274(5)	0.5	0.55(6)
H	4*g*	0.374(1)	0.0852(9)	0.5	1.8(1)

for the hydroxy arsenate compound are in good agreement with those of the $Co_2(OH)PO_4$ phase.[11,12]

B. Magnetic properties

Variable-temperature magnetic-susceptibility measurements between 1.8 and 300 K are represented in Fig. 4. The molar magnetic susceptibility shows a complex behavior with the presence of three different characteristic temperatures. First, χ_m increases as the temperature decreases from room temperature and reaches a rounded maximum at approximately 30 K. Below 19 K, a strong increase in magnetic signal with a new inflexion point close to 6 K appears.

The experimental data obey a classical Curie-Weiss law above 80 K with a extrapolated Curie temperature close to −62 K and an effective paramagnetic moment per formula unit (f.u.) of $\mu_{eff}=3.26\mu_B$. The negative Weiss temperature together with the decrease in the $\chi_m T$ vs T indicates that the major magnetic interactions in this compound are antiferromagnetic. The abrupt upturn of the susceptibility at $T_N \approx 19$ K corresponds to the onset of AF order, as will be described later from neutron powder-diffraction data. It should be noted that this behavior is clearly different from that described for the homologous $Co_2(OH)PO_4$ compound where the AF ordered appears at approximately 70 K.

The temperature dependence of ZFC-FC curves at 1 kOe does not show any difference above 15 K [see inset in Fig. 4]. Below this temperature, the curves show a small splitting attributed to the existence of a small ferromagnetic component in the $Co_2(OH)AsO_4$ compound. This magnetic irreversibility grows on increasing the applied field up to 20 kOe (Fig. 5). When the applied field is higher, the irreversibility decreases in intensity and almost disappears for a magnetic field of 90 kOe. Besides, the irreversibility temperature is strongly dependent on the magnetic field (from 12 K down to 5 K at fields of 0.5 kOe and 90 kOe, respectively).

As can be seen in Fig. 5, above 20 K, the ZFC is not affected by the external magnetic field. However, the inflection point at around 18.2 K for a field 1 kOe, attributed to the antiferromagnetic ordering, is moved when the magnetic field is increased to a temperature of 20.1 K for an applied field of 90 kOe [see inset in Fig. 5]. In addition, the inflexion point at around 6 K is transformed into a new and well-

TABLE III. Main interatomic distances (Å) and angles (deg) for $Co_2(OH)AsO_4$ (D2B, RT). Symmetry code: i=$\frac{1}{2}-x,y-\frac{1}{2},\frac{1}{2}-z$; ii=$\frac{1}{2}-x,\frac{1}{2}+y,\frac{1}{2}-z$; iii=$x-\frac{1}{2},\frac{1}{2}-y,z-\frac{1}{2}$; iv=$-x,-y,1-z$; v=$x-\frac{1}{2},\frac{1}{2}-y,\frac{1}{2}-z$; vi=$-x,-y,-z$; and vii=$x,y,-z$; viii=$x,y,1-z$.

Bond distances (Å)

$Co(2)O_4(OH)_2$ octahedron		$Co(1)O_4(OH)$ trigonal bipyramid	
Co(2)-O(2)^{i,iv}	2.070(9)×2	Co(1)-O(4)H	2.076(9)
Co(2)-O(4)H^{i,iv}	2.059(9)×2	Co(1)-O(1)^{ii}	2.072(9)
Co(2)-O(3)^{ii,iv}	2.222(2)×2	Co(1)-O(1)^{iii}	1.996(8)
		Co(1)-O(3)^{i,viii}	2.003(4)×2
AsO_4 tetrahedron			
As-O(1)		1.707(5)	
As-O(2)		1.703(5)	
As-O(3)^{i,viii}		1.683(3)×2	

Bond angles (deg)

$Co(2)O_4(OH)_2$ octahedron		$Co(1)O_4(OH)$ trigonal bipyramid	
O(2)-Co(2)-O(2)	84.8(9)	O(1)-Co(1)-O(1)	75.5(4)
O(2)-Co(2)-O(3)	96.5(3)×2	O(1)-Co(1)-O(3)	123.3(3)×2
	88.9(3)×2		95.4(4)×2
O(2)-Co(2)-O(4)H	94.7(3)×2	O(1)-Co(1)-O(4)H	89.7(4)
	170.8(4)×2		165.2(5)
O(3)-Co(2)-O(3)	172.5(2)	O(3)-Co(1)-O(3)	113.0(2)
O(3)-Co(2)-O(4)H	92.6(3)×2	O(3)-Co(1)-O(4)H	92.6(4)×2
	81.9(3)×2		
O(4)-Co(2)-O(4)H	87.0(4)		
AsO_4 tetrahedron			
O(1)-As-O(2)		104.0(4)	
O(1)-As-O(3)		110.4(3)×2	
O(2)-As-O(3)		112.7(3)×2	
O(3)-As-O(3)		106.5(2)	

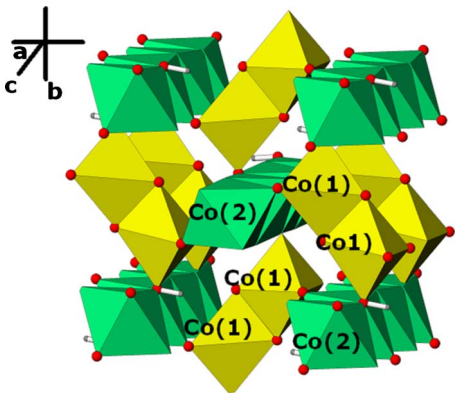

FIG. 3. (Color online) Partial polyhedral view of the packing of $Co_2(OH)AsO_4$ in the z direction. Tetrahedra have not been shown for clarity.

defined maximum when the magnetic field is 20 kOe, as their intensity subsequently decreases as the field increases.

Dependence on the magnetization with applied magnetic field at different temperatures has been represented in Fig. 6. As can be seen, at 2 K, the magnetization versus the applied field follows a process in stages characteristic of a metamagnetic transition. Up to 3.5 kOe, no magnetic irreversibility is observed while between 3.5 and 40 kOe, a small irreversibility appears with ΔH_{max} of 4.5 kOe (see inset figure of dM/dH). With increasing temperature, the magnetic irreversibility decreases, reaching a value of $\Delta H_{max}=1.5$ kOe at 10 K. Indeed, at 15 K, the magnetization still shows a weak metamagnetic transition at $H=12.5$ kOe but no irreversibility is observed. Finally, at 20 K, the magnetization curve shows a lineal behavior in the whole applied field range suggesting the absence of magnetic order. It is worth mentioning that the magnetic moment at 2 K and 90 kOe is quite different from the theoretical saturation magnetic moment for this compound ($3.4\mu_B$/mol), indicating the existence of a strong anisotropy. This general behavior is clearly different from that observed in the $Co_2(OH)PO_4$ compound in which the

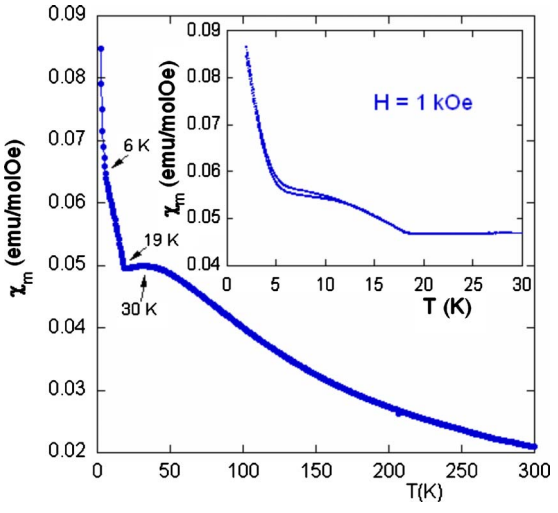

FIG. 4. (Color online) Thermal evolution of the molar magnetic susceptibility (χ_m) at 1 kOe for $Co_2(OH)AsO_4$. The inset shows low-temperature ZFC-FC measurements at 1 kOe.

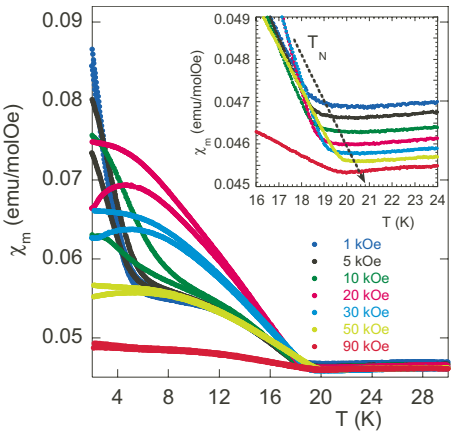

FIG. 5. (Color online) Low-field ZFC-FC magnetic susceptibility at difference fields. The inset shows the field dependence of the long-range ordering temperature.

hysteresis loop has a small coercitivity characteristic of spin glasses.[11]

The thermal evolution of the ac susceptibility at different magnetic fields is shown in Fig. 7. Three different temperature regions as described for the magnetic-susceptibility data can be observed: (i) the presence of a rounded maximum at around 30 K in the real (χ') component of the susceptibility which remains practically unchanged when applying magnetic field, (ii) the inflection point located on the real (χ') component of the susceptibility below 20 K, associated with long-range antiferromagnetic ordering. It becomes more defined (more three dimensional), moving toward higher temperatures as the applied magnetic field is increased (see inset in Fig. 7), reaching a value of 20.3 K at 90 kOe. The absence of signal in the imaginary (χ'') component of the susceptibility above 15 K confirms the origin of the antiferromagnetic ordering,[11] and (iii) the inflection point at around 6 K, in the real (χ') and imaginary (χ'') component of the susceptibility confirms that it turns into a maximum defined for an applied field of 5 kOe. This signal decreases in intensity, with shifts in temperature as the magnetic field increases becoming extinct in fields above 30 kOe.

The temperature dependence of the molar heat capacity (C_p) for $Co_2(OH)AsO_4$ is shown in Fig. 8. Calorimetric measurements in the absence of external magnetic field reveal a small maximum ($\Delta C_p=2$ J/Kmol) centred at 18.6 K (see upper inset in Fig. 8). This anomaly does not have the typical appearance of a second-order transition of λ but it can be associated with the establishment of a three-dimensional antiferromagnetic order in good arrangement with the magnetic-susceptibility data. Besides, no anomaly is observed below 10 K, which prompted us to propose that the magnetic contribution around 6 K observed in the magnetic-susceptibility measurements is not of a long-range type (implying a disordered magnetism). Above the peak, C_p increases continuously due to the phonon contribution and does not show any tendency to saturation even up to room temperature, where the value of C_p is 160 J/Kmol, still far from the expected value according to the Dulong and Petit law[23] (224.5 J/Kmol). This is due to the presence of light atoms with very high excitation energy.

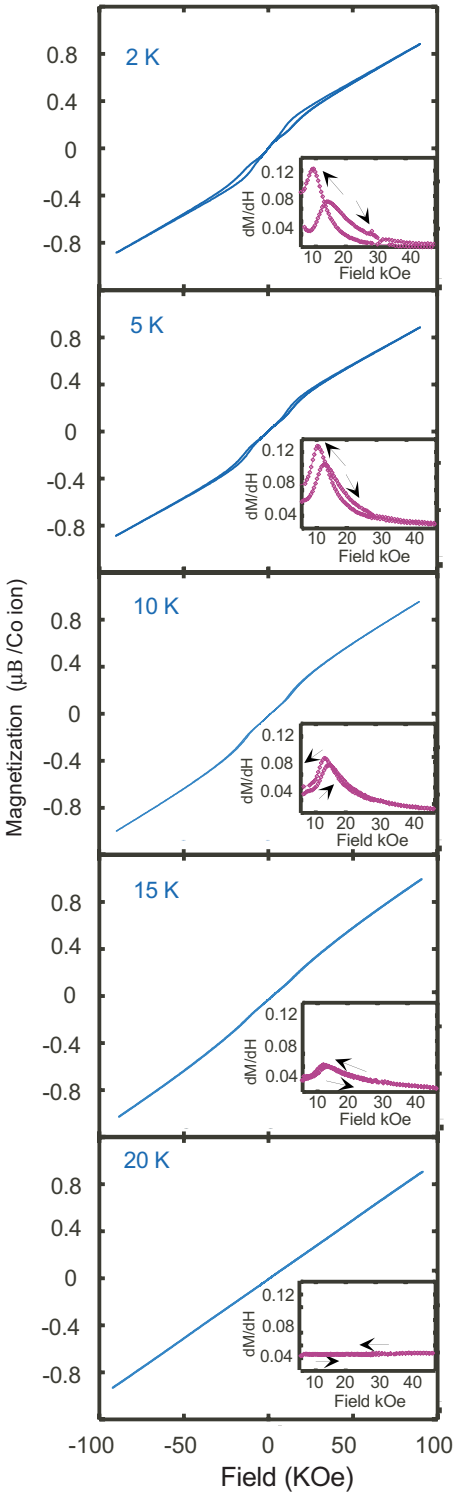

FIG. 6. (Color online) Magnetization vs applied magnetic field at different temperatures for $Co_2(OH)AsO_4$. The insets show the derivate of magnetization with magnetic field.

In order to extract the magnetic contribution (C_{mag}), that phonon (C_{pho}) should be determined. The exact calculation of C_{pho} is difficult due to the absence of a suitable nonmagnetic isomorphous compound. As it was satisfactorily used for $Co_2(OH)PO_4$,[11] an estimation of C_{pho} was obtained using the Debye model[24] and considering the existence of two Debye temperatures, the smaller one (θ_1) associated to the heavy ions such us Co and As (n_1) and the higher one (θ_2) associated to the O and H light ions ($9-n_1$). The best fit to the experimental data for $T \geq 60$ K is obtained for $\theta_1 = 270$ K, $\theta_2 = 1048$ K, and $n_1 = 3.6$ ions. The magnetic contribution (C_{mag}) with temperature dependence is shown in the lower inset of Fig. 8. Apart from the maximum associated with the three-dimensional magnetic order around 19 K, another anomaly like a shoulder circa 30 K is observed. This kind of broad maximum could come from different origins: (i) bidimensional magnetic ordering, (ii) short-range magnetic interactions, or (iii) a crystalline electrical field, as will be analyzed later in the discussion.

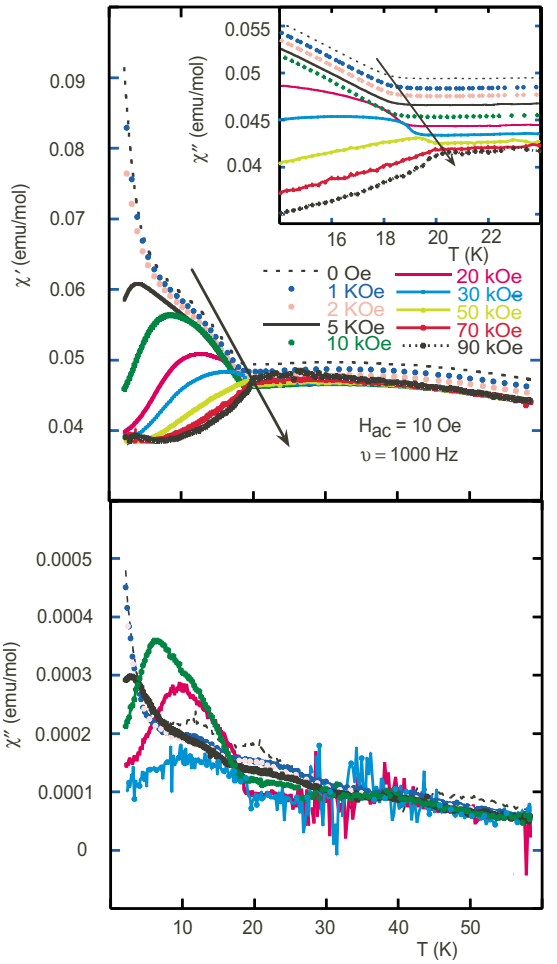

FIG. 7. (Color online) Thermal evolution of the ac susceptibility of $Co_2(OH)AsO_4$ at different dc applied fields with an ac field $H_{ac}=10$ Oe and frequency of 1000 Hz. The inset shows the frequency dependence of the long-range ordering temperature.

Heat-capacity measurements have been taken in the presence of several magnetic fields. Because the phonon contribution is not affected by the magnetic field, we have subtracted those values from the experimental data and obtained the magnetic contributions (see Fig. 9). Usually, the effects of the magnetic field on antiferromagnetic or ferromagnetic transition become more rounder (and decrease in height) the λ anomaly, shifting it to either low (antiferromagnetic) or high (ferromagnetic) temperatures. In our case, unexpectedly, the maximum associated to the three-dimensional or-

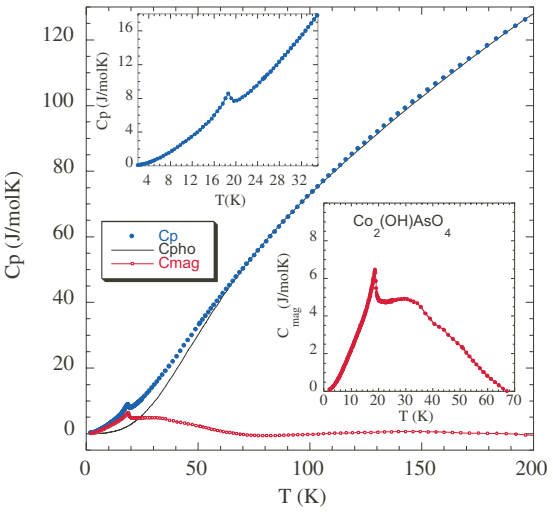

FIG. 8. (Color online) Specific heat of $Co_2(OH)AsO_4$ between 1.8 and 200 K. Experimental data (blue full dots), estimated phonon contribution (black full line), and magnetic contribution (red dots). Upper inset shows the experimental data and lower inset the magnetic contribution at low temperatures.

dering grows with field and becomes better defined (see upper inset of Fig. 9). These anomalous results will be explained later from neutron powder-diffraction data. In order to understand this surprising phenomenon, we have plotted the evolution of both, the temperature of the maximum and the temperature of the inflexion point above the maximum as a function of the applied magnetic field. Both magnitudes evolve in the same way: nearly constant up to 10 kOe, a sudden increase between 2 and 60 kOe and, finally a tendency to saturation above 80 kOe (see lower inset in Fig. 9).

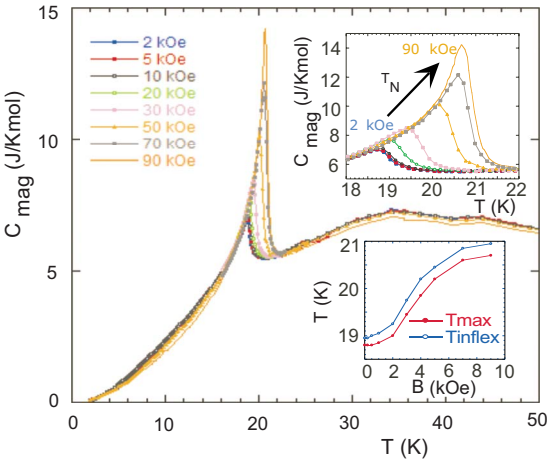

FIG. 9. (Color online) Magnetic specific heat as a function of temperature in the presence of external magnetic fields ($H \leq 90$ kOe) of $Co_2(OH)AsO_4$. The upper inset shows an enlargement around the Neel temperature and the lower inset the evolution of both, the temperature of the maximum and the temperature of the inflexion with the applied magnetic field.

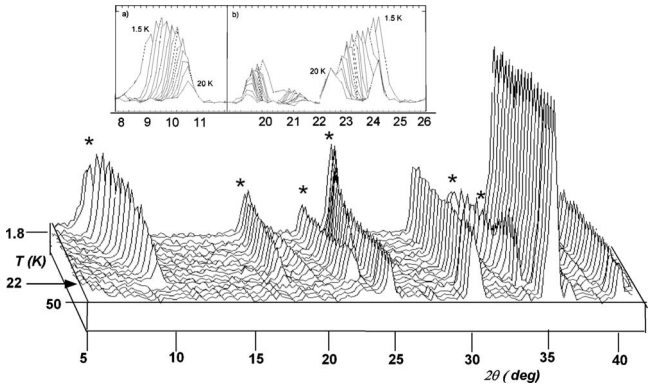

FIG. 10. Thermal evolution of the D1B patterns between 1.8 and 50 K. The (*) dots show the magnetic contributions. The inset shows the magnetic reflections (a) 0–10, ±100 and the neighbor (b) ±1–10 from 8° to 12° and 18° to 26°, respectively.

C. Low-temperature neutron diffraction

The thermal evolution of the D1B patterns is shown in Fig. 10. For the high-temperature NPD patterns, all the Bragg reflections can be indexed in the orthorhombic *Pnnm* space group. The refined lattice parameters at 50 K $a=8.241(8)$ Å, $b=8.564(8)$ Å, and $c=6.028(6)$ Å show a small shift with respect to the 300 K data [$a=8.258(1)$ Å, $b=8.580(1)$ Å, and $c=6.039(6)$ Å] due to effect of temperature. New peaks appear in the patterns with decreasing temperature below 25 K confirming the onset of a magnetic ordering with a T_N value of 21 K. These new peaks can be indexed with the propagation vector $\mathbf{k}=(0,\delta,0)$, indicating the existence of an incommensurate (IC) antiferromagnetic structure along the *b* direction. The modulation wave vector characterizing the oscillatory magnetic order is temperature dependent with a value of $(0,\delta,0)$, where $\delta=0.430$ at the lowest temperature (1.8 K) of these measurements. As can be seen in Fig. 10, the intensity of the magnetic reflections increases in a monotonous way below T_N and reaches saturation at low temperature. Presence of anomalies indicating a modification of the long-range spin arrangement was not observed.

The magnetic structure was solved by means of symmetry-representation analysis[25] using the program BASIREPS.[26] The possible representations were systematically checked with FULLPROF program.[21] After refining, the Fourier components of the atomic magnetic moments for each irreducible representation, a $\Gamma 1(00Gz)$ for site 4*b* and the mixing of ireps $\Gamma 2(00fz)$ and $\Gamma 3(00az)$ for site 4*g* were observed as the best solution (see symmetric analysis in Appendix). Rietveld refinements of this solution with a magnetic moment perpendicular to the propagation vector in the *z* direction gave a fully satisfactory fit (Fig. 11). Hence, Co^{2+} moments are ordered with the magnetic moment modulated in a longitudinal sinusoidal wave perpendicular to the propagation vector. This ordering is visualized in Fig. 12. The components of the refined magnetic moments of Co(1) and Co(2) are $2.81(1)\mu_B$ and $3.64(3)\mu_B$, respectively, with a resultant magnetic moment of $3.22(2)\mu_B$ per Co^{2+} ion. The nuclear and magnetic discrepancy factors are $R_p=16.1$, $R_{wp}=14.4$, $\chi^2=2.61$, $R_{Bragg}=6.9$, and $R_{mag}=14.4$.

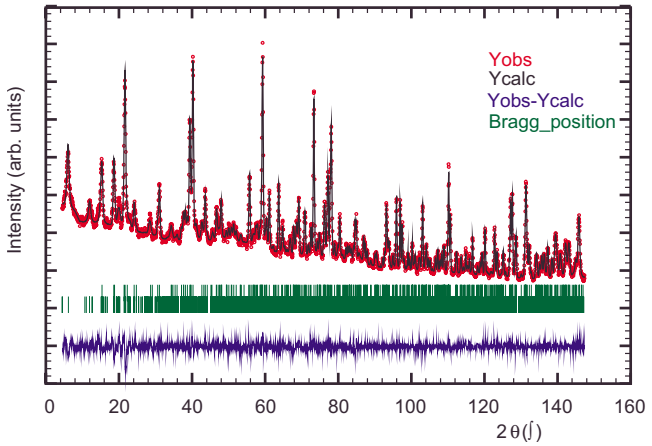

FIG. 11. (Color online) Neutron diffraction profiles of $Co_2(OH)AsO_4$ at 2 K obtained in D2B. Crosses are experimental, solid line calculated, and blue line differential data. First line of vertical marks corresponds to the position of the allowed reflexion for the crystallographic structure and the second line marks the magnetic reflexions.

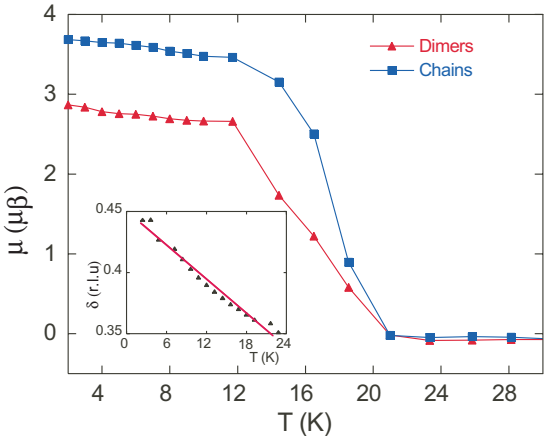

FIG. 13. (Color online) Magnetic moment for $Co_2(OH)AsO_4$ refined from neutron data obtained with D1B as a function of temperature for chains and dimers of the Co^{2+} ions. The inset shows the magnitude of the propagation vector $(0,\delta,0)$ as a function of temperature. Solid lines are only visual guidelines.

The magnetic moment was refined from the D1B data at all available temperatures. The nuclear structure and anisotropic temperature factors were kept from the refined D2B data at 2 K. The thermal dependence of the ordered magnetic moments is represented in Fig. 13. It can be observed that the three-dimensional magnetic order starts at 21 K, the ordering temperature being similar in both sublattices. The curves of the Co(1) and Co(2) moments rapidly increase from 21 K to approximately 15 K with a change in the slope at around 12 K (Fig. 13). The magnetic moment for the Co(1) and Co(2) ions in the dimer groups and chains slowly increases with practically linear variation from $2.64(4)\mu_B$ and $3.46(5)\mu_B$ at 12 K to $2.81(1)\mu_B$ and $3.64(3)\mu_B$ at 1.8 K. Furthermore, the refined magnetic moments of the Co(2) octahedral ions are always higher than those of the Co(1) trigonal bipyramidal geometry in the whole temperature range studied. In addition, the δ component of the magnetic propagation vector **k** continuously decreases with increasing temperature from 0.43 to 0.36 (see inset in Fig. 13).

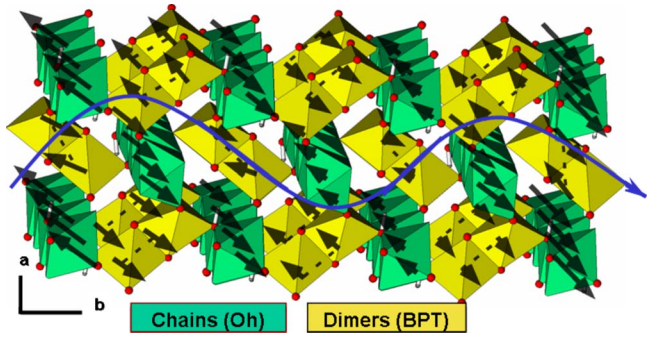

FIG. 12. (Color online) Incommensurate antiferromagnetic structure of $Co_2(OH)AsO_4$ along the *b* direction. The ordering of the magnetic moments of Co^{2+} is in *z* direction for three crystallographic unit cells for the two crystallographic positions (dimers and chains). The sinusoidal modulation of the magnetic moments is also shown. Note that at a given temperature (2 K), there is only one propagator vector but there may be differences of phases between the magnetic sites.

Neutron powder diffraction at different temperatures and fields were performed using a 50 kOe cryomagnet coupled to D2B diffractometer ($\lambda = 1.5938$ Å). During the field experiments, the high-intensity nuclear reflection (3, 2, 0) was measured repeatedly to control the correct orientation of the sample. In Fig. 14, we present the results from magnetic neutron diffraction with magnetic field at 1.5 K. In addition, we show the neutron diffraction of zero field and 25 K (paramagnetic state) for comparison.

We find that the propagation vector $\mathbf{k}(0,\delta,0)$ is highly dependent on the magnetic field between 0 and 35 kOe. At zero field, magnetic Bragg intensities can be detected at (0, 0.43, 0) originations from an incommensurate antiferromagnetic structure along the *b* direction (Fig. 11). When the magnetic field increases, the magnetic bragg reflections of IC phase continuously decrease in intensity and there appear new magnetic satellites that can be indexed with a propagation vector (0, 0.33, 0). At 35 kOe, a sudden drop in all incommensurate peak intensities, denoting the transition of the magnetic structure into collinear AF magnetic phase (Fig. 15). The new increase in the magnetic field (50 kOe) produces significant changes in the magnetic intensities but not in the peak positions of the magnetic phase (Fig. 14). This is a result of the increase in the magnetic ordering of commensurable structure in good agreement with the surprising phenomenon observed in specific-heat data.

As can be observed in Fig. 16, the applied magnetic field up to 50 kOe does not change the value of the ordering temperature. However, for values higher than 30 kOe, the external magnetic field seems to overcome the competing interactions that give rise to the incommensurate ordering. A magnetic phase transition takes place as a function of the magnetic field to a commensurate structure with propagation vector (0, 0.33, 0). The resolution of this commensurate structure is under way.

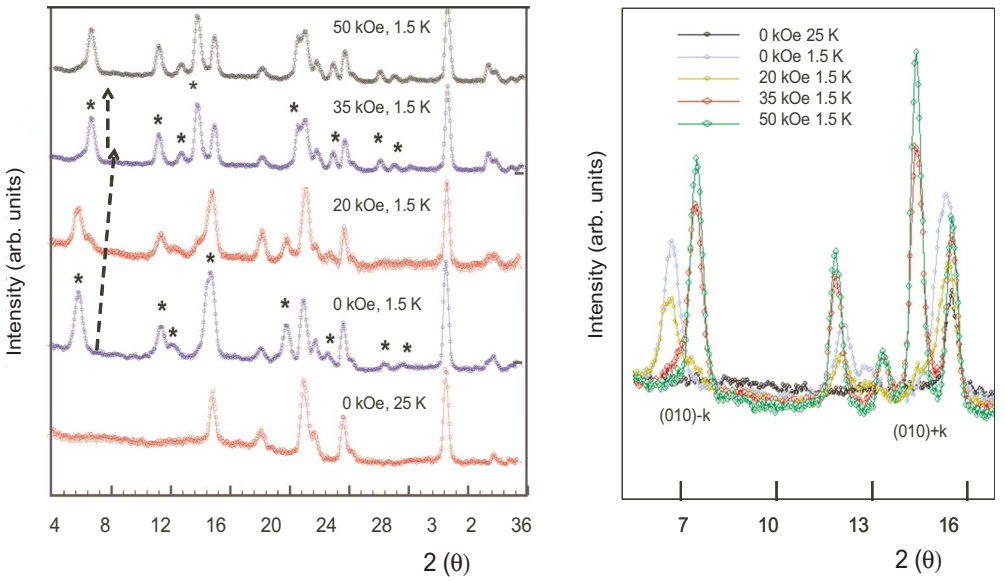

FIG. 14. (Color online) (Left) Evolution of the neutron-diffraction peaks of $Co_2(OH)AsO_4$ at different fields at 1.5 K obtained in D2B compared with the zero field and 25 K. (Left) Magnetic peaks are marked with * sign. Step narrows are visual guidelines for the eyes showing the shift of the (010)-*k* peak. (Right) Enlargement of the low angle diffraction.

IV. DISCUSSION AND CONCLUSIONS

The magnetic behavior of $Co_2(OH)AsO_4$ shows the presence of two types of magnetic interactions: (i) three-dimensional antiferromagnetic interactions dominating at high temperatures, which are those responsible for the high extrapolated negative Curie-Weiss temperature and (ii) ferromagnetic interactions at temperatures lower than 15 K, where the field-cooled magnetization increases. This fact can be explained as due to the existence of ferromagnetic interactions in an overall antiferromagnetic behavior which predominates at high temperatures.

The dependence of the magnetization with applied magnetic field follows a process in stages characteristic of a metamagnetic transition below 19 K. The value of the magnetic moment at 2 K and 90 kOe is far below the theoretical saturation magnetic moment for this compound ($3.4\mu_B$/mol), indicating the existence of a strong anisotropy. The magnetic irreversibility in ZFC-FC curves grows on increasing the applied field up to 20 kOe and almost disappears for a magnetic field of 90 kOe. In addition, the inflexion point at around 6 K, observed at 1 kOe, is transformed into a new and well-defined maximum when the magnetic field is

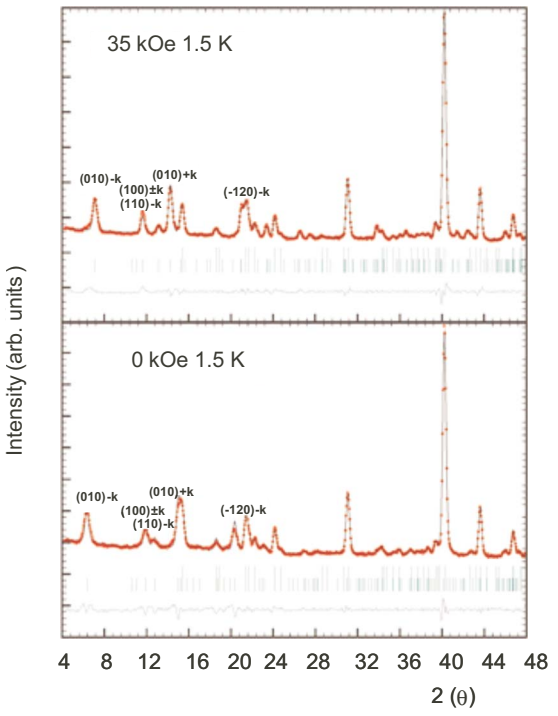

FIG. 15. (Color online) Neutron diffraction profiles of $Co_2(OH)AsO_4$ at 0 and 35 kOe obtained in D2B. Crosses are experimental, solid line calculated, and blue line differential data. First line of vertical marks corresponds to the position of the allowed reflexions for the crystallographic structure and the second line marks the magnetic reflexions.

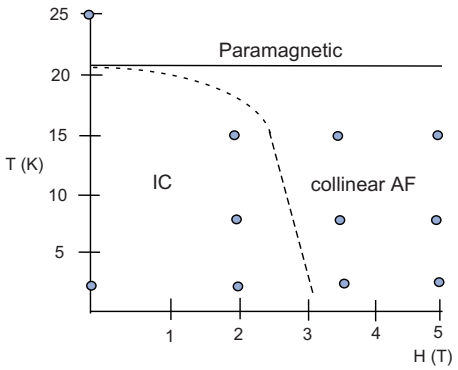

FIG. 16. (Color online) Magnetic phase diagram of $Co_2(OH)AsO_4$. Blue circles are neutron diffraction obtained in D2B. The thin broken curve marks a boundary where different magnetic phases could not be resolved in the diffraction pattern.

20 kOe. The fit of the magnetic data to a Brillouin law[27] at different fields in this region of temperature indicates the nonexistence of magnetic impurities (see supplementary material).

Three-dimensional antiferromagnetic ordering between Co^{2+} ions appears at around 20 K, showing an unusual magnetic behavior with the magnetic field. The inflection point on magnetic-susceptibility data, associated with long-range antiferromagnetic ordering, becomes more defined (more three dimensional), moving toward higher temperatures ($\approx$2 K) as the applied field increases. Besides, regards heat-capacity data, another unusual effect with the magnetic field is observed. The maximum associated to the three-dimensional ordering grows with the field, becoming better defined. This behavior can be explained as an incommensurate-commensurate magnetic phase transition with the magnetic field.

Another anomaly appears at approximately 30 K as a rounded maximum or shoulder in magnetic-susceptibility and C_{mag} data, respectively. The nonappearance of anomalies in this region of temperature in powder-diffraction data indicates the absence of long-range spin arrangement. This signal is not affected by the external magnetic field and it could be originated by the existence of bidimensional magnetic order, the presence of short-range magnetic interactions or crystalline electrical field.

The possible existence of a bidimensional magnetic order precursor to the three-dimensional ordering circa 30 K could be analyzed from the magnetic heat-capacity data with quasi-two-dimensional antiferromagnetic Heisenberg models with varying interplanar couplings,[28]

$$C_v^{3D} = C_v - C_v^{plane} = C_v^{inter} + C_v^{cross}.$$

The purely interplane contribution C_v^{inter} and cross term C_v^{cross} are given by

$$C_v^{inter} = [\langle n_z^2\rangle - \langle n_z\rangle^2 - \langle n_z\rangle]/N,$$

$$C_v^{cross} = 2[\langle n_p - n_z\rangle - \langle n_p\rangle\langle n_z\rangle]/N,$$

where n are the numbers of bond operators in the expansion acting within a single layer (n_p) and between two layers (n_z) and N is the system of size.

The comparison of the experimental magnetic heat capacity of $Co_2(OH)AsO_4$ with the theoretical model shows a good agreement (Fig. 17), where correlations between two-dimensional coupling constants (shoulder width to 30 K) are lower than the dimensional coupling constants (peak at 19 K).

Another possibility is the presence of short-range magnetic interactions. However, the fit of the magnetic-susceptibility data at 1 kOe above 25 K to a classical bidimensional model gave negative results. Besides, until now, an adequate theoretical model to study these types of interactions in heat-capacity data has been not described despite the presence of compounds that show similar magnetic behavior.[29]

Finally, we have also considered the possible effect of the crystalline electrical field (C_{CEF}) on the magnetic contribution in this temperature region. Theoretical calculations[30] indicated that the hexacoordinated Co(II) ion presents a low quadruplet separated by an energy Δ_1 from the first excited doublet whereas in the pentacoordinated Co(II) ion, the lower levels are two doublets separated by an energy Δ_2. The addition of these two contributions ($C_{pho}+C_{CEF}$) to the heat capacity, fits the experimental data above the ordering temperature quite well (Fig. 18). The best fit is obtained for values of θ_1=299 K, θ_2=1057 K, n_1=3.7, Δ_1=80 K, and Δ_2=85 K, respectively. Therefore, from these results, we can conclude that all contributions proposed to explain the magnetic anomaly at approximately 30 K should be taken into consideration.

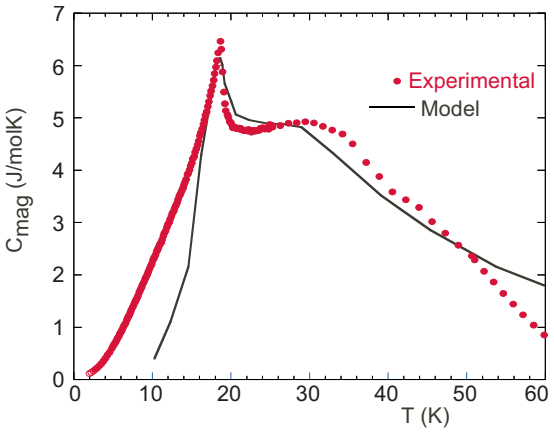

FIG. 17. (Color online) Comparison of the experimental magnetic heat capacity of $Co_2(OH)AsO_4$ (red) with the theoretical model for anisotropic Heisenberg antiferromagnetic system (see text).

The incommensurate magnetic structures are characterized by modulations of their spin arrangements over periods which are long compared to the size of the chemical cell and not commensurate with the underlying lattice.[31] In our case, the $Co_2(OH)AsO_4$ phase shows an incommensurate antifer-

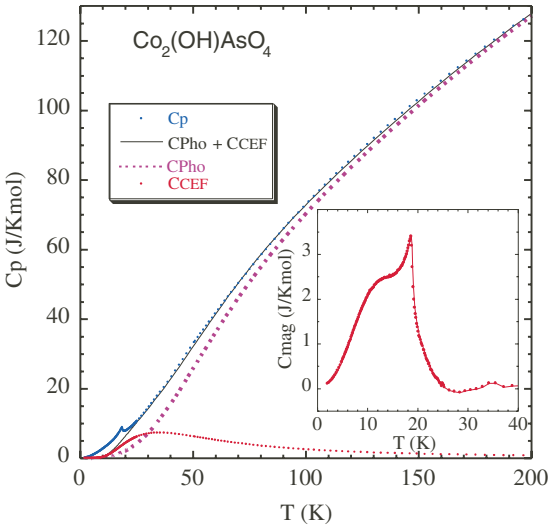

FIG. 18. (Color online) Specific heat of $Co_2(OH)AsO_4$ between 1.8 and 200 K. Experimental data (blue full dots), estimated phonon contribution and crystal-field effect (C_{CEF}) (blank full line), and magnetic contribution (red dots).

TABLE IV. Selected geometrical parameters, bond lengths (Å), and angles (deg) related to the possible magnetic superexchange pathways for $Co_2(OH)XO_4$ (X=P and As). The data were obtained from D2B.

Direct and through bonding distances, Co-Co (Å)					
	As	P		As	P
Co(1)-O(1)-Co(1)	3.22	3.24	Co(1)-O(1)-Co(1)	4.11	4.07
Co(1)-O(1)-*X*-O(3)-Co(1)	5.48	5.49	Co(1)-O(1)-*X*-O(3)-Co(1)	7.47	7.21
Co(1)-O(4)H-Co(2)	3.62	3.65	Co(1)-O(4)H-Co(2)	4.05	4.02
Co(1)-O(3)-Co(2)	3.59	3.55	Co(1)-O(3)-Co(2)	4.23	4.45
Co(1)-O(3)-*X*-O(2)-Co(2)	5.59	5.64	Co(1)-O(3)-*X*-O(2)-Co(2)	7.52	7.22
Co(2)-O(4)H-Co(2)	2.90	2.99	Co(2)-O(4)H-Co(2)	4.04	4.04
Co(2)-O(2)-Co(2)	3.13	3.04	Co(2)-O(2)-Co(2)	4.18	4.12
Co(2)-O(2)-*X*-O(3)-Co(2)	5.95	6.05	Co(2)-O(2)-*X*-O(3)-Co(2)	7.72	7.61

Length of exchange pathway								
	Angles (deg)							
	Co-O-Co		Co-O-*X*		O-*X*-O		*X*-O-Co	
	As	P	As	P	As	P	As	P
Co(1)-O(1)-Co(1)	103.0	101.6						
Co(1)-O(1)-P-O(3)-Co(1)			125.6	133.0	110.2	110.2	126.0	131.0
Co(1)-O(4)H-Co(2)	126.2	123.2						
Co(1)-O(3)-Co(2)	116.9	107.0						
Co(1)-O(3)-P-O(2)-Co(2)			126.6	125.0	112.0	110.2	122.0	127.0
Co(2)-O(4)H-Co(2)	91.7	92.4						
Co(2)-O(2)-Co(2)	97.2	92.1						
Co(2)-O(2)−*X*-O(3)-Co(2)			122.0	128.6	112.0	110.2	116.0	112.0

romagnetic structure along the b direction below 22 K with the propagation vector $(0,\delta,0)$ temperature dependent, will δ=0.430 being he value at the lowest temperature (1.8 K).

The magnetic structure of $Co_2(OH)AsO_4$ consists of ferromagnetic arrangements between the Co(2) octahedral chains and Co(1) trigonal bipyramidal dimers along the c-axis-modulated antiferromagnetic between subnets in direction b (Fig. 12). The magnetic interactions in each sublattice, $[Co(2)O8]_\infty$ octahedral chains, and $[Co(1)_2O8]$ dimeric units, together with the interactions through the $|OH^-|$ and arsenate groups give rise to a three-dimensional antiferromagnetic coupling in good agreement with the results obtained from the magnetic measurements. Electronic paramagnetic resonance and reflectance diffuse spectroscopies indicate that only Co^{2+} ions are present in this phase.[30,32] In this way, the markedly different saturated magnetic moments in $Co_2(OH)AsO_4$ with two chemically similar Co^{2+} cations must be based on the differences between the geometries around the two cation sites. Spontaneous static ordering of the magnetic moments at low temperatures is caused by exchange interactions between the moments, making it energetically favorable for them to align, either parallel or antiparallel.

If we consider the commensurate AF structure of the isomorphous $Co_2(OH)PO_4$ phase,[11] the appearance of an amplitude modulated by changing the PO_4^{3-} for AsO_4^{3-} anions demonstrated the strong anisotropy magnetocristalline present in these $Co_2(OH)XO_4$ (X=P and As) phases. The main magnetic exchange pathways present in these isomorphous compounds are shown in Table IV and Fig. 19. The shorter Co-Co distances range between 2.9 and 3.65 Å and consequently direct interactions are not negligible. Ferromagnetic couplings are observed in the superexchange Co-O-Co interactions in both the edge-sharing $[Co(1)_2O_6(OH)_2]$ trigonal bipyramidal dimers and $[Co(2)O_4(OH)_2]$ octahedral chains whose angles range from 91.7° to 103.0° leading to

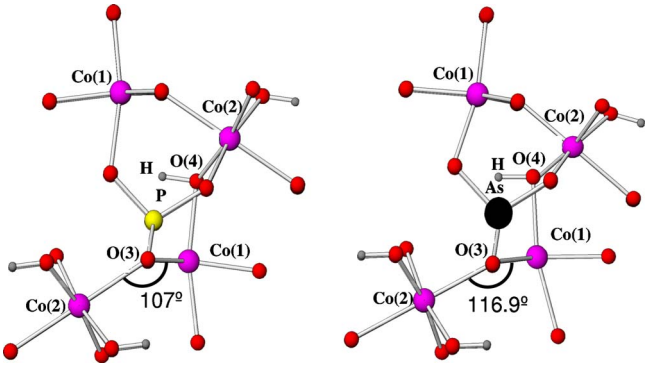

FIG. 19. (Color online) Schematic view of the exchange pathways for $Co_2(OH)XO_4$ (X=P and As). Interactions via vertex oxygen bridges of the phosphate and arsenate groups.

TABLE V. Irreducible representations (ireps) for the group of the propagation vector $\mathbf{G_k k}=\mathbf{k_y b}^*(k_y<1/2)$ in the space group *Pnnm*.

				Basis functions vectors, $S(\nu,\mathbf{k},\lambda\|j)$ for $4b$ site						Basis functions vectors, $S(\nu,\mathbf{k},\lambda\|j)$ for $4g$ site					
Γ_ν	1	n	n	m	S_1	S_2	S_3	S_4		R_1	R_2		R_3	R_4	
Γ_1	1	$-w$	$-w$		(100)	$(-w00)$	(-100)	$(w00)$	A_x						
					(010)	$(0w0)$	$(0-10)$	$(0-w0)$	C_y						
					(001)	$(00-w)$	(001)	$(00-w)$	G_z	(001)	$(00w)$	f_x	$(00w)$	(001)	f_x
Γ_2	1				(100)	$(-w00)$	(100)	$(-w00)$	G_x	(100)	$(w00)$	f_x	$(w00)$	(100)	f_x
					(010)	$(0w0)$	(010)	$(0w0)$	F_y	(010)	$(0w0)$	a_y	$(0w0)$	(010)	a_y
					(001)	$(00-w)$	$(00-1)$	$(00w)$	A_z						
Γ_3	1				(100)	$(w00)$	(-100)	$(-w00)$	C_x						
					(010)	$(0-w0)$	$(0-10)$	$(0w0)$	A_y						
					(001)	$(00w)$	(001)	$(00w)$	F_z	(001)	$(00-w)$	a_z	$(00w)$	$(00-1)$	a_z
Γ_4	1				(100)	$(w00)$	(100)	$(w00)$	F_x	(100)	$(-w00)$	a_x	$(w00)$	(-100)	a_x
					(010)	$(0-w0)$	(010)	$(0-w0)$	G_y	(010)	$(0w0)$	f_y	$(0w0)$	(010)	f_y
					(001)	$(00w)$	$(00-1)$	$(00-w)$	C_z						

ferromagnetic interactions in both compounds. On the other hand, superexchange interactions Co(1)-O(4)H-Co(2) (Fig. 19) with a mean exchange angle of 123.2° and 126.2° for phosphate and arsenate, respectively, give rise to antiferromagnetic couplings.

It is worth mentioning the comparison of the magnetic exchange interaction, Co(1)-O(3)-Co(2), between dimers and their neighbor chains in the $Co_2(OH)XO_4$ (X=P and As) phases (Table IV and Fig. 19). In this way, in the phosphate phase, this magnetic exchange has a striking angle of 107° (for ferromagnetic interactions through the xz plane) which was considered essential in the competition between dimers and chains in order to ensure cooperativeness of the freezing process associated to a spin-glass state of this phase.[11] However, the substitution of the PO_4^{3-} by AsO_4^{3-} anions modifies substantially the magnetic exchange Co(1)-O(3)-Co(2) angle from 107° to 116.9° for the phosphate and arsenate, respectively, relaxing the magnetic frustration system of $Co_2(OH)PO_4$ leading to an incommensurate phase with antiferromagnetic interactions (sinusoidal amplitude modulated) in $Co_2(OH)AsO_4$ (Fig. 13). Finally, the magnetic interactions propagated via $|XO_4|$ tetrahedra (X=P,As) characterized by both the O-X-O and X-O-Co angles give rise to a three-dimensional antiferromagnetic coupling.

In summary, the obtained results indicate the existence of an anomalous three-dimensional antiferromagnetic ordering influenced by the magnetic field in the $Co_2(OH)AsO_4$ phase. The presence of both the strong anisotropy of the Co(II) ions and the magnetic frustration in the Co(1) and the neighboring Co(2) sublattices could be responsible for the complex magnetic behavior observed in this compound. Besides, an incommensurate-commensurate magnetic phase transition from IC to collinear commensurate antiferromagnetic state can explain the unusual magnetic properties observed in this compound.

ACKNOWLEDGMENTS

This work was financially supported by the Universidad del País Vasco/EHU (UPV/EHU) under Grant No. GIU06/11 and by MEC research under Projects No. MAT 2007-66737-c02-01 and No. MAT 2008-06542-c04).

APPENDIX

Symmetry analysis

In order to determine the magnetic structure of the $Co_2(OH)AsO_4$, it is very important to classify the possible spin configurations according to the irreducible representations (ireps) of the space group for the propagation vector. For $Co_2(OH)AsO_4$, all the magnetic reflections can be indexed using a propagation vector $\mathbf{k}=ky\mathbf{b}^*$ with $ky<1/2$. Symmetry analysis for space group *Pnnm* with this kind of propagation vector has previously been performed for the $4b$ position, obtaining the different basis functions of the ireps describing the magnetic ordering at this site.[33] The extended analysis for all magnetic sites and their final results are summarized in Table V. For $Co_2(OH)AsO_4$, the center of symmetry is lost. The coset representatives of $\mathbf{G_k}$ are (x,y,z); $(-x+1/2,y+1/2,-z+1/2)$; $(x,y,-z)$; $(-x+1/2,y+1/2,z-1/2)$. There are four one-dimensional irreducible representations. The basis functions of positions $4b$ (named S) and $4g$ (named R) are also given. We have used an extension to complex basis functions with the Bertaut notations[34] for the modes F, A, C, and G. The value of w is $e^{i\pi k}y$. The numbering of atoms in the $4b$ site is $S_1(0,0,z)$; $S_2(-x+1/2,y+1/2,-z+1/2)$; $S_3(x,y,-z+1)$; and $S_4(-x+1/2,y+1/2,z+1/2)$ with $z\approx 0.2597$. The atoms in the $4g$ site split in two orbits previously related by the center of symmetry having the same basic functions. The coupling between these two orbits is usually positive or negative but in the general case, there is a phase factor between them. The cobalt atoms of the first orbit are $R_1(x,y,1/2)$; $R_2(-x+1/2,y+1/2,-z+1/2)$ and those of the second orbit: $R_3(1-x,1-y,1/2)$; $R_4(-x+3/2,y-1/2,-z+1/2)$, with $x\approx 0.3642$ and $y\approx 0.3645$. The symbols (f, a) used to describe the basis functions for the Co orbits correspond for F and A for a two-atoms orbit.

The decomposition of the full reducible magnetic representation Γ (of dimension three times the number of atoms in the primitive cell) for $4b$ is $\Gamma_{4b}=\Sigma \pm n_\nu \Gamma_\nu = 3\Gamma_1 \pm 3\Gamma_2 \pm 3\Gamma_3 \pm 3\Gamma_4$, the corresponding decomposition for the two $4g$ sites is $\Gamma_{4g1,4g2}=\Gamma_1 \pm 2\Gamma_2 \pm \Gamma_3 \pm 2\Gamma_4$. The number of free parameters for a magnetic structure corresponding to an irep is equal to the product ($n_{\text{free}}=n_\nu d_\nu$) of the number of times (n_ν) the irep Γ_ν n is contained in Γ and the dimension (d_ν) of the irep. This is also the total number of independent basis function vectors.

The magnetic moment of the atom "j," in the cell with origin at the lattice point $\mathbf{R}_n$, in a magnetic structure characterized by the set of propagation vectors $\{\mathbf{k}\}$, is given by the Fourier series, $\mathbf{m}_{nj}=\Sigma_{\{\mathbf{k}\}}\mathbf{S}_{\mathbf{k}j}e^{2\pi \mathbf{k}i\mathbf{R}n}$, where the sum is extended to the whole set of propagation vectors. For $\mathbf{k}$ at the interior of the Brillouin zone, the vector $-\mathbf{k}$ should also be present and $\mathbf{S}_{\mathbf{k}j}=\mathbf{S}^*_{\mathbf{k}j}$. The physical meaning of the basis functions of the irep Γ_ν in describing a magnetic structure is that the Fourier coefficients $\mathbf{S}_{\mathbf{k}j}$ are linear combinations of the constant vectors $\mathbf{S}\ \alpha(\mathbf{k},\upsilon,\lambda|j)$ so that

$$S_{\mathrm{K}j}=\Sigma_\alpha C_\alpha S_\alpha(\nu,\mathbf{k},\lambda|j).$$

For a given propagation vector $\mathbf{k}$ and a given irep $\Gamma_\nu n$, the index α runs between 1 and n_ν and λ between 1 and d_ν (for details, see Ref. 25). The coefficients $C_{\alpha\lambda}$ can be real or purely imaginary. By varying these coefficients, we obtain the whole class of magnetic structures satisfying the symmetry of the propagation vector. Let us consider two examples for the cobalt sublattices constructed with the representation Γ_3. The irep is of dimension 1 (so $\lambda=1$ and the summation index over λ is therefore removed) and it is contained three times in Γ_{4b} so the number of coefficients is 3 ($\alpha=1,2,3$). The possible magnetic structures described by this irepare given by

$$S_{\mathrm{K}1}=\Sigma_\alpha C_\alpha S_\alpha(\nu,\mathbf{k},1|1)=C_1(1,0,0)+C_2(0,1,0)+C_3(0,0,1)=(C_1,C_2,C_3),$$

$$S_{\mathrm{K}2}=\Sigma_\alpha C_\alpha S_\alpha(\nu,\mathbf{k},1|2)=C_1(w,0,0)+C_2(0,-w,0)+C_3(0,0,w)=w(C_1,-C_2,C_3),$$

$$S_{\mathrm{K}3}=\Sigma_\alpha C_\alpha S_\alpha(\nu,\mathbf{k},1|3)=C_1(-1,0,0)+C_2(0,-1,0)+C_3(0,0,1)=(-C_1,-C_2,C_3),$$

$$S_{\mathrm{K}4}=\Sigma_\alpha C_\alpha S_\alpha(\nu,\mathbf{k},1|4)=C_1(-w,0,0)+C_2(0,w,0)+C_3(0,0,w)=w(-C_1,C_2,C_3).$$

If, e.g., $C_1=C_3=0$, the structure corresponds to a collinear longitudinal sinusoidal structure. If $C_2=0$, and $C_1=iC_3$ with C_3 purely imaginary, the structure corresponds to a helix with a cylindrical envelope. If $C_1=0$ and $C_2=iC_3$ the structure is a cycloid, etc.

To solve the magnetic structure, one has to look for the set of coefficients that give rise to the best agreement between observed and calculated magnetic intensities. This part of the analysis may be undertaken simply by trial and error, by hand or using Monte Carlo techniques.

*teo.rojo@ehu.es

[1] S. Agrestini, L. C. Chapon, A. Daoud-Aladine, J. Schefer, A. Gukasov, C. Mazzoli, M. R. Lees, and O. A. Petrenko, Phys. Rev. Lett. **101**, 097207 (2008).

[2] R. D. Adams, R. Layland, C. Payen, and T. Datta, Inorg. Chem. **35**, 3492 (1996).

[3] S. Kobayashi, S. Mitsuda, M. Ishikawa, K. Miyatani, and K. Kohn, Phys. Rev. B **60**, 3331 (1999).

[4] Z. He, J. I. Yamaura, Y. Ueda, and W. Cheng, J. Am. Chem. Soc. **131**, 7554 (2009).

[5] Z. He, D. Fu, T. Kyömen, T. Taniyama, and M. Itoh, Chem. Mater. **17**, 2924 (2005).

[6] Z. He, T. Taniyama, T. Kyömen, and M. Itoh, Phys. Rev. B **72**, 172403 (2005).

[7] T. Kanazawa, *Inorganic Phosphate Materials* (Elsevier Science, Amsterdam, 1989).

[8] R. C. Haushalter and L. A. Mundi, Chem. Mater. **4**, 31 (1992); A. Clearfield, Chem. Rev. **88**, 125 (1988).

[9] W. R. Rapoport and C. P. Khattaak, Appl. Opt. **27**, 2677 (1988); G. T. Forrest, Laser Focus World **25**, 23 (1989).

[10] J. M. Rojo, J. L. Mesa, R. Calvo, L. Lezama, R. Olazcuaga, and T. Rojo, J. Solid State Chem. **145**, 629 (1999).

[11] J. M. Rojo, J. L. Mesa, L. Lezama, J. L. Pizarro, M. I. Arriortua, J. Rodriguez Fernandez, G. E. Barberis, and T. Rojo, Phys. Rev. B **66**, 094406 (2002).

[12] W. T. A. Harrison, J. T. Vaughey, L. L. Dussack, A. J. Jacobson, T. E. Martin, and G. D. Stucky, J. Solid State Chem. **114**, 151 (1995).

[13] P. Keller, H. Hess, and F. Zettler, Neues Jahrb. Mineral. Abh. **134**, 147 (1979).

[14] I. de Pedro, J. M. Rojo, J. L. Pizarro, J. Rodríguez Fernández, J. Sánchez Marcos, M. T. Fernández-Diaz, M. I. Arriortua, and T. Rojo, J. Phys.: Condens. Matter **18**, 3767 (2006).

[15] I. de Pedro, J. M. Rojo, J. L. Pizarro, J. Rodríguez Fernández, J. Sánchez Marcos, M. T. Fernández-Diaz, M. I. Arriortua, and T. Rojo, J. Mater. Chem. **17**, 3915 (2007).

[16] A. A. Belik, H. J. Koo, M. H. Whangbo, N. Tsujji, P. Naumov, and E. Takayama-Mourachi, Inorg. Chem. **46**, 8684 (2007).

[17] I. de Pedro, J. M. Rojo, L. Lezama, and T. Rojo, Z. Anorg. Allg. Chem. **633**, 1847 (2007).

[18] F. C. Hawthorne, Can. Mineral. **14**, 143 (1976).

[19] R. J. Hill, Am. Mineral. **61**, 979 (1976).

[20] J. M. Rojo, J. L. Mesa, J. L. Pizarro, L. Lezama, M. I. Arriortua, and T. Rojo, Mater. Res. Bull. **31**, 925 (1996).

[21] J. Rodríguez-Carvajal, Physica B **192**, 55 (1993) and later unpublished versions; the program is a strongly modified version of that described by D. B. Wiles and R. A. Young, J. Appl. Crystallogr. **14**, 149 (1981).

[22] H. M. Rietveld, J. Appl. Crystallogr. **2**, 65 (1969).

[23] A. T. Petit and P. L. Dulong, Ann. Chim. Phys. **10**, 395 (1819).

[24] P. Debye, Ann. Phys. **344**, 789 (1912).
[25] Y. A. Izymov, V. E. Naish, and R. P. Ozerov, *Neutron Diffraction of Magnetic Materials* (Consultants Bureau, New York, 1991).
[26] J. Rodríguez-Carvajal, BASIREPS, ftp://ftp.cea.fr/pub/llb/divers/BasIreps
[27] B. D. Cullity, *Introduction to Magnetic Materials* (Addison-Wesley, Reading, MA, 1972).
[28] P. Sengupta, A. W. Sandvik, and R. R. P. Singh, Phys. Rev. B **68**, 094423 (2003).
[29] A. M. Durand, P. Klavins, and L. R. Curruccini, J. Phys.: Condens. Matter **20**, 235208 (2008); A. Yaouanc, P. Dalmas de Reotier, V. Glazkov, C. Marin, P. Bonville, J. A. Hodges, P. C. M. Gubbens, S. Sakarya, and C. Baines, Phys. Rev. Lett. **95**, 047203 (2005).
[30] M. E. Foglio, M. C. dos Santos, G. E. Barberis, J. M. Rojo, J. L. Mesa, L. Lezama, and T. Rojo, J. Phys.: Condens. Matter **14**, 2025 (2002).
[31] T. Chattopadhyay, Science **264**, 226 (1994).
[32] I. de Pedro, J. M. Rojo, J. Rodríguez Fernández, L. Lezama, and T. Rojo, Eur. J. Inorg. Chem. (to be published).
[33] J. Rosset-Mignod, in *Methods of Experimental Physics: Neutron Scattering*, edited by K. Skold and D. L. Price (Academic, New York, 1987), Vol. 23C.
[34] E. F. Bertaut, Acta Crystallogr., Sect. A: Cryst. Phys., Diffr., Theor. Gen. Crystallogr. **24**, 217 (1968).